Advancing electrical properties through hybridization: Synthesis, characterization, and doping of poly(maminophenol)/

Advancing Electrical Properties through Hybridization: Synthesis, Characterization, and Doping of Poly(m-aminophenol)/SnO_2Nanocomposites

Bouabdellah Daho[1], Abdelkader Dehbi[1,*], Ali Alsalme[2], Giovanna Colucci[3]and Massimo Messori[3]

[1] *Engineering Physics Laboratory, University of Tiaret, Tiaret, 14000 Algeria.*

[2]*Department of Chemistry, College of Science, King Saud University, Riyadh 11451, Saudi Arabia.*

[3] *Department of Applied Science and Technology (DISAT), Politecnico di Torino, CorsoDucadegli Abruzzi 24, 10129 Torino, Italy*

*Corresponding author: *DehbiAbdelkader, Email:* abddehbi@gmail.com

Abstract

This study focuses on the synthesis of novel organic/inorganic hybrid materials by combining the conductive polymer poly (m-aminophenol) (PMAP) with the metal oxide SnO_2, with the primary aim of enhancing the electrical properties of the resulting nanocomposite polymer. The nanocomposite is intricately crafted through in situ polymerization of m-aminophenol in the presence of SnO_2, incorporating various loading rates (1%, 3%, 10%). Comprehensive characterization of the synthesized materials is conducted using analytical techniques including infrared spectroscopy (IR), UV-Visible spectroscopy, and X-ray diffraction (DRX), confirming the structural integrity of the hybrid materials. Notably, XRD analyses distinctly illustrate the successful integration of SnO_2 into the polymer matrix. Conducting an extensive study on the doping of PMAP samples with varying concentrations of SnO_2 (1%, 3%, and 10%) reveals a nuanced relationship between dopant concentration and electrical conductivity. The doped polymers exhibit a significant enhancement in electrical conductivity, directly correlating with the concentration of SnO_2. This comprehensive exploration offers valuable insights into customizing the electrical properties of hybrid materials for diverse applications.

Key words: poly (m-aminophenol), nanocomposites, tin oxide, electrical properties.

INTRODUCTION

Conducting polymers have emerged as a focal point of scientific and technological exploration in recent years, garnering substantial interest due to their diverse and promising applications. Within this extensive field, a considerable share of research has been dedicated to polyaniline (PANI), a member of the broad family of polymers derived from the oxidative electrochemical or chemical polymerization of aniline or its derivatives. PANI and its various derivatives exhibit remarkable electronic and electro-conductive properties, positioning them as versatile materials with applications spanning a wide array of fields [1–6]. The synthesis and exploration of these polymers open up possibilities for innovations in electronic and conductive materials, paving the way for advancements in areas such as sensors, energy storage, and electronic devices. The multifaceted nature of PANI underscores its significance as a cornerstone in the ongoing quest for novel materials with tailored functionalities.

The formidable challenge in the technological utilization of polyaniline (PANI) arises from its inherently low solubility. The unsubstituted PANI in salt form demonstrates insolubility in common organic solvents. However, the landscape changes with substituted PANI derivatives, such as poly(o-toluidine), poly(o-anisidine), poly(aniline-co-o-nitroaniline), and poly(aniline-co-o-anisidine), which exhibit enhanced solubility compared to their unsubstituted counterpart [7–9]. The growing interest in conjugated polyaminoarenes, including PANI and its derivatives, is primarily fueled by their improved solubility and holds immense potential for technological applications in chemical power sources and electrochromic displays [10]. Of particular note, aminophenols stand out as intriguing electrochemical materials. In contrast to aniline and other substituted anilines, aminophenols possess two distinct groups ($–NH_2$ and –OH) susceptible to oxidation. This dual functionality enables them to exhibit electrochemical behavior reminiscent of both anilines [11–13] and phenols [14, 15]. The unique electrochemical properties of aminophenols render them captivating candidates for various applications, making them particularly appealing in the realm of sensor technology.

In recent years, there has been a substantial surge in research focused on the polymerization of o-, m-, and p-aminophenol [16–20]. The extensive literature on the subject indicates that poly(o-, m-, p-aminophenol) tends to exhibit greater solubility than unsubstituted polyaniline (PANI) in common organic solvents. Notably, m-aminophenol (3-amino phenol) (MAP) follows a polymerization process akin to that of aniline. Typically, the chemical polymerization of MAP is accomplished in acidic solutions, employing oxidizing agents such as ammonium

peroxydisulphate (APS) [21–23]. This methodology has proven effective in facilitating the synthesis of polymerized m-aminophenol, paving the way for the exploration of its unique properties and potential applications. The soluble nature of poly(m-aminophenol) positions it as a promising candidate for diverse applications, and the utilization of APS as an oxidant agent adds a layer of versatility to the synthesis process.

In recent times, there has been a burgeoning interest in the development of nanoscale inorganic/polymer hybrid materials, fueled by the vast array of potential applications they offer [24-27]. These nanocomposite materials have swiftly become the focus of extensive global research, showcasing their versatility and applicability in a myriad of technological domains. Notably, they have demonstrated significant promise in the realm of effective quantum electronic devices, magnetic recording materials, and sensors, contributing to the evolution of cutting-edge technologies [28]. Furthermore, the synergy achieved in nanocomposite materials comprising conducting polymers and oxides has opened up new avenues for applications, extending beyond traditional boundaries. This class of materials has found utility in diverse fields, including drug delivery systems, conductive paints, rechargeable batteries, toners in photocopying, smart windows, and more [29, 30]. The multifaceted nature of these inorganic/polymer hybrid nanocomposites positions them as pivotal contributors to technological advancements across various industries. Tin oxide (SnO2) nanoparticles (NPs) are undergoing development for a spectrum of applications, spanning from their use as an opacifier in ceramic glazes to cutting-edge technologies such as gas sensors, lithium-ion batteries, low-emission window coatings, touch screens, sensitized solar cells, field emission flat displays, and various optoelectronic devices [31]. Across these diverse applications, the imperative is to establish a straightforward, cost-effective, and scalable synthesis approach capable of generating NPs with a narrow size distribution [32].

In previous work, a new mixed organic semiconductor material was synthesized from Poly(benzaldehyde-co-thiophene)/SnO_2 Composites. The study of the electrical and optical properties of this compound comfirms this. [33]

In the course of this investigation, the synthesis of poly(meta-aminophenol) (PMAP) was accomplished through a chemical method ~~employing~~ that employed ammonium peroxydisulphate (APS) as the oxidant [34-38]. Simultaneously, the fabrication of PMAP/SnO2 composites were fabricated using a conventional in situ chemical oxidative polymerization process [38-42]. This process entailed the polymerization of meta-aminophenol (MAP) in the presence of SnO_2 particles. The resultant polymer samples underwent comprehensive

characterization utilizing a range of analytical techniques, including Fourier-transform infrared spectroscopy (FTIR), UV–visible spectroscopy (UV–vis), and x-ray diffraction (XRD). FTIR spectroscopy provided insights into the molecular structure and functional groups present in the synthesized materials, while UV–visible spectroscopy offered information on their optical properties. Concurrently, XRD analyses were crucial in elucidating the crystalline structure and confirming the successful integration of SnO_2 particles within the polymer matrix. These characterization techniques collectively contribute to a comprehensive understanding of the composition, structure, and properties of the synthesized PMAP and PMAP/SnO_2 composites. The electrical conductivity and activation energy of the composites were evaluated using an LCR-meter apparatus.

2. MATERIALS AND METHODS

The synthesis of poly(meta-aminophenol) was conducted in an acidic medium using a standard procedure. The monomer, m-aminophenol (m-AP), was initiated the through gradual addition of the oxidizing agent, ammonium peroxydisulphate (APS), and concentrated H2SO4 served as a dopant. This process occurred under continuous stirring at a temperature range of 0-5°C. Maintaining a monomer to oxidizing agent ratio of 1:1, with 4.18 units of m-AP were combined with 4.56 units of APS. After the complete addition of the oxidizing agent, the reaction mixture underwent continuous stirring for 4 hours. Subsequently, the resulting product was filtered and washed with distilled water until the filtrate became colorless. Finally, the polymer was dried and processed into a powdered form, successfully synthesizing poly(meta-aminophenol).

The tin dioxide nanoparticles were synthesized using the sol–gel method [43]. In a standard procedure, 8.35g of hydrated tin chloride ($SnCl_2 \cdot 2H_2O$) was dissolved in 100ml of pure ethanol (C_2H_5OH). The resulting solution underwent a magnetic stirring for 30 minutes in a closed three-necked flask. Subsequently, the solution was continuously refluxed at 80°C for 2 hours to generate the SnO_2 sol solution. Prior to the calcination process at 650°C for 1 hour, the sol was dried at 100°C for 30 minutes, resulting in the formation of well-defined tin dioxide nanoparticles. This method ensures the controlled synthesis of SnO_2 nanoparticles through the precise formation of the sol and subsequent controlled calcination, providing a reproducible and effective route for their preparation.

The poly(m-aminophenol)/SnO_2 composites were fabricated through an in situ chemical oxidative polymerization process of the m-aminophenol (m-AP) monomer in the presence of

SnO_2 particles. Initially, SnO_2 particles were dispersed in 50 mL of chloroform under ultrasonic vibrations at room temperature for 10 minutes. Subsequently, m-AP (3.27 g, 10 mmol) was introduced into different weight percentages (1%, 3% and 10% wt) of the SnO_2 dispersion in 50 ml of 1N H2SO4 under vigorous stirring.

Concurrently, 10.27 g (15 mmol) of ammonium peroxydisulphate (APS) was dissolved in 50 ml of 1N H_2SO_4. The aqueous APS solution was then added drop by drop to the m-AP solution, and the entire mixture was continuously stirred for 30 minutes. The reaction took place in an ice bath for 4 hours. Throughout the process, the color of the mixture transformed from gray to a deep black hue, indicating the successful polymerization and the formation of poly(m-aminophenol)/SnO_2 composites.

The solubility of PMAP was assessed using various solvents. A 20 mg powder sample of the polymer was introduced into 10 mL of each solvent, including water, chloroform, diethyl ether, and dimethyl sulfoxide (DMSO). The mixture was meticulously dispersed. Subsequently, the mixture underwent continuous stirring at room temperature, allowing for the examination and determination of the polymer's solubility in each solvent. This approach provides valuable insights into the polymer's compatibility with different solvents, aiding in the understanding of its potential applications and handling characteristics.

The X-ray diffraction (XRD) patterns for the samples were acquired under ambient conditions utilizing a Philips X-ray powder diffractometer with Cu Kα radiation (λ = 1.5406 Å). Scans were conducted at a rate of 2°/min within the angular range of 20–80°. Fourier-transformed infrared (FTIR) spectra were obtained using a Jasco FT/IR-4200 (ATR) spectrometer employing the KBr pellet method. Furthermore, the ultraviolet–visible (UV–vis) characterization of PMAP and PMAP/SnO_2, spanning the region of 200–1000 nm, was performed on samples dissolved in DMSO using a (SHIMADZU 1650 PC) double-beam UV–vis spectrophotometer.

The temperature dependence of the dielectric and the electrical conductivity was investigated on pressed pellets (∅ = 13 mm, thickness ~ 0.8 mm), at 1V in a sandwich configuration with GW-Instek 821- LCR meter. The temperature was varied in the range of 300–373 K, with a heating rate of 4°C/min. All the measurements were recorded at fixed frequencies (100 kHz).

3. Results and discussion

The FTIR spectra of PMAP, as depicted in Fig. 1, reveal distinctive bands indicative of various molecular vibrations. Notably, the bands in the range of 600 to 810 cm^{-1} can be ascribed to the deformation vibration of the aromatic =C-H bonds. The peak observed at 1050 $cm^{-1}$is attributed to the stretching vibrations of the C-O-C bonds, a characteristic feature associated with the transformation of precursor materials, including meta-aminophenol, into the polymer PMAP. Furthermore, the vibrational band at 1283 cm^{-1} corresponds to the C-N bond of the aromatic amine, suggesting the establishment of a C-N-C structure within the polymer matrix.

Additionally, the presence of bands spanning from 1500 cm^{-1} to 1585 cm^{-1} signifies vibrations associated with the C=N and C=C double bonds, providing further insights into the structural composition of PMAP. Notably, a broadband extending from 2500 cm^{-1} to 3700 $cm^{-1}$is observed, indicating the amalgamation of two absorption bands related to the stretching vibrations of –OH, $–NH_2$, and the aromatic groups –CH. This spectral information contributes to a comprehensive understanding of the molecular composition and bonding arrangements present in the synthesized PMAP polymer.

The UV-Vis spectra of PMAP, as depicted in Fig. 2 and recorded in DMSO, offer valuable insights into the electronic transitions within the synthesized polymer. The initial absorption band, manifesting itself around 280 nm, is attributed to the $\pi - \pi^*$ transition of the benzenoid ring. This distinctive absorption feature is intimately linked to the degree of conjugation exhibited by the phenyl rings along the polymer chain. The position of this absorption band provides crucial information about the extent of electron delocalization within the aromatic system of the polymer. In the case of PMAP, the absorption at 280 nm signifies the involvement of the benzenoid moieties in π-electron interactions, indicating the presence of an extended conjugated system~~,~~ this information is pivotal for understanding the electronic structure and optical properties of the synthesized polymer.

In our analysis of the absorption spectra, we employed the Tauc method [44] to ascertain the Tauc difference (E_{Tauc}). This involved extrapolating the intense absorption region towards lower energies, utilizing the relationship $(\alpha.h\nu)^{1/2} = f(h\nu)$, where α represents the absorption coefficient determined by the expression: $\alpha = 2.303A/d$. The gap energy, determined through linear extrapolation for PMAP and PMAP/SnO_2at room temperature, ~~as~~ is illustrated in Fig. 3. The calculated energy gap serves as a key parameter in characterizing the electronic properties of the material. In the case of PMAP, the determined gap of 2.31 eV suggests that the polymer possesses a bandgap within the semiconductor range. The results, presented in Table 1, show that the optical gap energy of PMAP is 2.31 eV, while the PMAP/SnO_2 composites have lower

gap energies, ranging from 2 eV to 2.09 eV, depending on the doping rate of SnO_2 (see Figure 3). Specifically, the gap energy decreases with increasing doping rate from 0 to 10%.

The diffractogram of PMAP, as illustrated in Fig. 4, exhibits a distinctive pattern characterized by diffuse and broadened lines. This unique diffraction profile is a clear indication of the presence of disordered zones within the polymer structure. The observation of diffuse lines in the diffractogram is a characteristic feature associated with materials that possess an amorphous structure. In the case of poly(m-aminophenol) or PMAP, the amorphous nature is evident from the absence of sharp, well-defined diffraction peaks that would typically indicate a crystalline structure. The existence of disordered zones and the overall amorphous nature of PMAP are critical aspects influencing its material properties. Amorphous polymers often exhibit advantageous characteristics, such as enhanced solubility and processability, making them suitable for various applications, including coatings, adhesives, and certain types of sensors. Diffractogram analysis, therefore, provides valuable insights into the structural arrangement of PMAP, guiding our understanding of its potential applications and informing future research directions aimed at optimizing its properties for specific uses.

The identification of the crystalline phases within tin dioxide powder, calcined at 650°C, was conducted across a scanning range from 3° to 80°. The analysis of the diffractogram presented in Figure 5 reveals distinct lines corresponding to the planes (110), (101), (200), (211), (220), (310), and (301). These observations align with the characteristic diffraction pattern of tetragonal tin dioxide, as documented in the JCPDS Powder Diffraction File Card 5-0467. The preferential orientation of these lines along the [111] plane further signifies the crystalline nature of the tin dioxide phase.

Upon examining the X-ray diffractogram of the PMAP/1%SnO_2, PMAP/3%SnO_2, and PMAP/10%SnO_2nanocomposites, as depicted in Figure 6, three prominent peaks at 25°, 35°, and 53° emerge conspicuously. These peaks align precisely with the characteristic diffraction peaks of SnO_2, providing clear evidence for the presence of tin dioxide particles within the PMAP matrix. The discernible peaks at specific angles substantiate the successful incorporation of SnO_2 into the nanocomposite structures, offering valuable insights into the crystalline phases and confirming the effective integration of SnO_2 within the PMAP matrix.

The measured electrical conductivity values are systematically outlined in Table 2. The Arrhenius curves, elucidating the logarithmic conductivity versus the reciprocal temperature, are depicted in Figure. 7 for both PMAP and its composite, PMAP/SiO_2. These curves, obtained

at a fixed frequency of 100 kHz and a power of 1000 mV, exhibit a linear trend, adhering to the principles of the Arrhenius law. Notably, a pronounced augmentation in electrical conductivity is discernible as the temperature of the studied samples rises. This observed increase in conductivity underscores the temperature-dependency of the electrical properties, highlighting the potential for tailored applications that leverage the dynamic behavior of these materials with varying temperatures.

$$\sigma = \sigma_0 e\left(-\frac{E_a}{K_B T}\right) \quad \text{Eq 1}$$

where σ_0 is a constant, E_a is the activation energy, k_B is the Boltzmann's constant and T is the temperature in Kelvin.

As the temperature rises, there is a notable increase in electrical conductivity, indicating that an elevated temperature enables charge carriers to surpass the activation energy barrier, thereby contributing to enhanced electrical conductivity. The activation energy (E_a) values, crucial for understanding this phenomenon, are determined by linearizing Eq. (1) and are presented in Table 1. It is noteworthy that the Ea values exhibit a range from 8.58×10^{-2} to 9.579×10^{-5} eV, with a consistent trend of decrease in activation energy upon the addition of SnO_2.

The Arrhenius curve illustrates the electrical conductivity of PMAP, revealing a baseline conductivity of 9.80×10^{-4} S cm^{-1}, which significantly surpasses that of polythiophene (approximately 10^{-7} S cm^{-1}) [45]. Furthermore, the introduction of SnO_2 results in a remarkable enhancement, with the electrical conductivity reaching 1.78×10^{-3} S cm^{-1} when the polymer contains 10% SnO_2. This substantial increase underscores the positive impact of SnO_2 as a dopant on the electrical performance of the polymer.

The activation energy values acquired align with typical values observed in organic semiconductors, as demonstrated by Thambidurai et al. [46]. As depicted in Table 1, the noticeable decrease in activation energy with the introduction of doping (SnO_2) correlates directly with the concurrent increase in conductivity. This relationship underscores the influence of SnO_2 doping on reducing the energy barrier for charge carriers, facilitating improved electrical conductivity, in line with established trends observed in organic semiconductor studies.

4. Conclusion

In conclusion, our study focused on the synthesis and characterization of nanocomposites comprising poly(m-aminophenol) (PMAP) and tin dioxide (SnO2) using an in-situ chemical polymerization technique with varying tin dioxide charge rates (1%, 3%, 10%). Solubility tests revealed that PMAP exhibits slight soluble in dimethyl sulfoxide (DMSO). Optical characterization indicated a semiconductor character in the MAP polymer. X-ray diffraction (XRD) analysis unveiled the amorphous nature of PMAP and the semi-crystalline structure of PMAP/SnO2 nanocomposites, where distinctive SnO2 peaks confirmed the successful tin oxide incorporation into the polymer matrix. The investigation into the doping of PMAP samples with varying concentrations of SnO_2 (1%, 3%, and 10%) unveils a nuanced relationship between dopant concentration and electrical conductivity. The doped polymers demonstrate a notable enhancement in electrical conductivity from 9.80×10^{-4} S $cm^{-1}$to 1.78×10^{-3} S cm^{-1}, with the extent of improvement correlating with the SnO_2 concentration. Moreover, the study highlights that the incorporation of SnO2 contributes not only to enhanced electrical properties but also to a general improvement in thermal stability. The doped polymers exhibit heightened resistance to thermal degradation, signifying a positive impact on their overall stability under varying temperature conditions. This dual enhancement in electrical conductivity and thermal stability positions SnO_2-doped polymers as promising materials for applications requiring robust performance in diverse environmental conditions.

Acknowledgment

The authors would like to acknowledge the Researchers Supporting Project (RSP-2023R78), King Saud University, Riyadh, Saudi Arabia.

Funding and/or Conflicts of interests/Competing interests.

Compliance with ethical standards

Conflict of interest: They have no conflict of interest

Funding : No funding

References

[1] Sharma AL, Saxena V, Annapoorni S, Malhotra BD. Synthesis and characterization of a copolymer: poly(anilineco-fluoroaniline). J. Appl. Polym. Sci. 2001;81:1460–1466.

[2] Herrasti P, Recio FJ, Ocón P, Fatás E. Effect of the polymer layers and bilayers on the corrosion behaviour of mild steel: comparison with polymers containing Zn microparticles. Prog. Org. Coat. 2005;54:285–291.

[3] Ivanov S, Mokreva P, Tsakova V, Terlemezyan L. Electrochemical and surface structural characterization of chemically and electrochemically synthesized polyaniline coating. Thin Solid Films. 2003;441:44–49.

[4] Jeevananda T, Siddaramaiah, Seetharamu S, Saravanan S, D'Souza L. Synthesis and characterization of poly(anilineco- acrylonitrile) using organic benzoyl peroxide by inverted emulsion method. Synth. Met. 2004;140:247–260.

[5] Borole DD, Kapadi UR, Mahulikar PP, Hundiwale DG. Influence of TiO2 and SiO2 on electrochemical, optical and electrical conductivity of polyaniline, poly(o-toluidine) and their co-polymer. Des. Mon. Polym. 2009;12:523–532.

[6] Özdemir C, Kaplan Can H, Çolak N, Güner A. Synthesis, characterization, and comparison of self-doped, doped, and undoped forms of polyaniline, poly(o-anisidine), and poly [aniline-co-(o-anisidine)]. J. Appl. Polym. Sci. 2006;99: 2182–2192.

[7] Gui Li X, Xia Wang L, Rong Huang M, Quing Lu Y, Fang Zhu M, Menner A, Springer J. Synthesis and characterization of pyrrole and anisidine copolymers. Polymer. 2001;42:6095–6103.

[8] Roy BC, Gupta MD, Bhoumik L, Ray JK. Spectroscopic investigation of water-soluble polyaniline copolymers. Synth. Met. 2002;130:27–33.

[9] Yalçınkaya S, Çolak N. Synthesis and characterization of poly(Aniline-co-o-Aminoaniline). Des. Monomers Polym. 2012;15:147–157.

[10] Konopelnyk OI, Aksimentyeva OI, Tsizh BR, Chokhan MI. Physical and technological properties of the sensor materials based on conjugated polyaminoarenes. Phys. Chem. Solid State. 2007;8:786–90.

[11] Stephanie C. Remke, Tobias H. Bürgin, Lucie Ludvíková, Dominik Heger, Oliver S. Wenger, Urs von Gunten, Silvio Canonica Water Research. Volume 213, 15 April 2022, 118095

[12] P.R. Erickson, N. Walpen, J.J. Guerard, S.N. Eustis, J.S. Arey, K. McNeill. Controlling factors in the rates of oxidation of anilines and phenols by triplet methylene blue in aqueous solution. J. Phys. Chem. A, 119 (13) (2015), pp. 3233-3243.

[13] Long, H., Chen, T.-S., Song, J., Zhu, S. & Xu, H.-C. Electrochemical aromatic C−H hydroxylation in continuous flow. Nat. Commun. 13, 3945−3951 (2022).

[14] Anderson, K. W., Ikawa, T., Tundel, R. E. & Buchwald, S. L. The selective reaction of aryl halides with KOH: synthesis of phenols, aromatic ethers, and benzofurans. J. Am. Chem. Soc. 128, 10694−10695 (2006).

[15] Xiong, W., Shi, Q. & Liu, W. H. Simple and practical conversion of benzoic acids to phenols at room temperature. J. Am. Chem. Soc. 144, 15894−15902 (2022).

[16] Ivanov VD, Zhuzhel'skii DV, Malev VV. Comparison of properties of aniline and o-aminophenol polymers obtained using hydrogen peroxide. Russ. J. Electrochem. 2008;44:1204–1211.

[17] Bereket G, Duran B. Anticorrosive properties of electrosynthesized poly(m-aminophenol) on copper from aqueous phenylphosphonic acid solution. Prog. Org. Coat. 2009; 64:57–66.

[18] Kar P, Pradhan NC, Adhikari B. A novel route for the synthesis of processable conducting poly(m-aminophenol). Mater. Chem. Phys. 2008;111:59–64.

[19] Kar P, Pradhan NC, Adhikari B. Induced doping by sodium ion in poly(m-aminophenol) through the functional groups. Synth. Met. 2010;160:1524–1529.

[20] Kong Y, Zhou Y, Shan X, Jiang Y, Yao C. Electropolymerization of m-aminophenol on expanded graphite and its electrochemical properties. Synth. Met. 2011;161: 2301–2305.

[21] Zhang J, Shan D, Mu S. A promising copolymer of aniline and m-aminophenol: chemical preparation, novel electric propertis and characterization. Polymer. 2007;48: 1269–1275.

[22] Kar P, Pradhan NC, Adhikari B. Effect on structure, processability, and conductivity of poly(m-aminophenol) of the initial acidity/basicity of the polymerization medium. J. Macromol. Sci. Part B. 2010;49:669–679.

[23] Kar P, Behera AK, Adhikari B, Pradhan NC. Optimization for the chemical synthesis of conducting poly (m-aminophenol) in HCl using ammonium persulfate. High Perform. Polym. 2010;22:428–441.

[24] A. A. Ebnalwaled, A. Yousef, M. K. Gerges, and A. Thabet, "Synthesis of Nano-Polyimide for Microelectronic Applications" Journal of Applied Chemical Science International, Issue 1, Vol. 6, pp.18-30, Jan., 2016.

[25] A. Thabet, and A.A. Ebnalwaled," Improvement of surface energy properties of PVC nanocomposites for enhancing electrical applications", Journal of the International Measurement Confederation (IMEKO), Elsevier, Vol. 110, Pages 78-83, Nov. 2017.

[26] A. Thabet, and A.A. Ebnalwaled," Controlling on attraction forces of water droplets on surfaces of polypropylene nanocomposites coatings" Transactions on Electrical and Electronic Materials Journal, Vol.19, Issue 5, pp. 387 - 395, Oct. 2018.

[27] Ahmed Thabet, "Emerging Nanotechnology Applications in Electrical Engineering" IGI Global, Publisher of Timely Knowledge, ISBN13: 9781799885368, ISBN10: 1799885364, EISBN13: 9781799885382, ISBN13 Softcover: 9781799885375, DOI: 10.4018/978-1-7998-8536-8, Pages 318, June 2021.

[28] Anderson A, Hunderi O and Granqvist , *J. Appl. Phys*., **1980,** 57,75

[29] Jarjayes O, Fries P H and Bidan G ,*Synthetic metals* , **1995**, 69,343

[30] Butter worth M D, Corradi R, Johal J, Lascelles S F, Maeda S, and Armes S.P , J Colloid Interface sci., 1995, 174,510.

[31] Kamat, P. V. Dominance of Metal Oxides in the Era of Nanotechnology. J. Phys. Chem. Lett.2011,2, 839−840.

[32] Chen, Z.; Pan, D.; Li, Z.; Jiao, Z.; Wu, M.; Shek, C.-H.; Wu, C.M. L.; Lai, J. K. L. Recent Advances in Tin Dioxide Materials: SomeDevelopments in Thin Films, Nanowires, and Nanorods.Chem. Rev.2014,114, 7442−7486.

[33]: Baleh, H., Bouazza, A., Benhaoua, C., Bassaid, S., Dehbi, A.and Belfedal, A. Polym. Sci. - A, 63(6),872-878 (2021).

[34]: Daho, B., Fontanesi, C., Messori, M., Dehbi, A. and Belfedal.A,.Semicond. 53(12), 1656-1664 (2019).

[35] Bassaid S, Benhaoua C, Taleb M, Sahli M, and Dehbi A, Composites 63 (3), 1 (2021).

[36] Baleh H, Dehbi A, Bassaid S, Belfedal A, Alsalme A, Messori M. Journal of Polymer Research 30 (7), 285 (2023).

[37] Bouazza A, Bassaid S, Dehbi A, Guarnaccio A, D'Auria M. Reaction Kinetics, Mechanisms and Catalysis 136 (3), 1589-1605. (2023).

[38] Bouazza A, Bassaid S, Dehbi A, Hadj-Zoubir N, Alsalme A, Robert D. Reaction Kinetics, Mechanisms and Catalysis, 136, 1625–1641 (2023).

[39] Bekri, I., Gherras, H., Dehbi, A. et al. Preparation and Characterization of New Soluble and Thermally Stable Polyazomethine by Polycondensation of Thiophene-2,5-dicarboxaldehyde and Ortho-tolidine for Optoelectronics. Polym. Sci. Ser. B (2023).

[40] Laoufi, M., Yahiaoui, A., Hachemaoui, A. et al. Synthesis and characterization of PPDMB poly (pyrrole-co-3,5-dimethoxybenzaldehyde) and PPMB poly (pyrrole-co-2-methoxybenzaldehyde): a new copolymer for solar cells. Colloid Polym Sci 300, 1139–1154 (2022).

[41] Fatima El Zohra Aris, Hachemaouia, A., Yahiaoui, A. et al. Synthesis, Characterization, and Microbial Degradation Behavior of Hydrogel Based on Poly(ε-caprolactone) and Methacrylic Anhydride. Polym. Sci. Ser. B 64, 417–428 (2022).

[42] Leila Mouacher, Yahiaoui, A., Hachemaoui, A. et al. Synthesis and Characterization of Conducting Poly(2-aminothiazole)/Modified-Clay Nanocomposites. Polym. Sci. Ser. B 63, 314–321 (2021)

[43] Madzlan Aziz n, Saad Saber Abbas, Wan Rosemaria Wan Baharo. Size-controlled synthesis of SnO2 nanoparticles by sol–gel method. Materials Letters 91 (2013) 31–34

[44] J. Tauc and A. Meuth, J. Non-Cryst. Solids 8-10, 569 (1972).

[45] N. E. H. Bouabida, A. Hachemaoui, A. Yahiaoui, H. Gherras, A. Belfedal, A. Dehbi, and A. H. I. Mourad, Polym. Sci., Ser. B 62, 163 (2020).

[46] M. Thambidurai, Foo Shini, Jun Young Kim, Changhee Lee, Cuong Dang. Materials Letters. Volume 274, 1 September 2020, 128003.

Table 1: Optical gap energy of PBT and composites

Materials	Optical gap energy (eV)
PMAP	2.31
PMAp /1% SnO_2	2.09
PMAP/3% SnO_2	2.06
PMAP /10% SnO_2	2.00

Table 2: The electrical properties of PMAP and PMAP/SnO_2 with different ration (1% SnO_2, 3% SnO_2 and 10%SnO_2)

Samples	**Conductivity at 300K ($S.cm^{-1}$)**	**Activation energy E_a (eV)**
PMAP	9.8e-04	8.6e-02
PMAP -1% SnO_2	1.1e-03	6.9e-05
PMAP- 3% SnO_2	1.5e-03	8.9e-05
PMAP-10 % SnO_2	1.8e-03	9.6e-05

Figure 1: FTIR spectra of PMAP

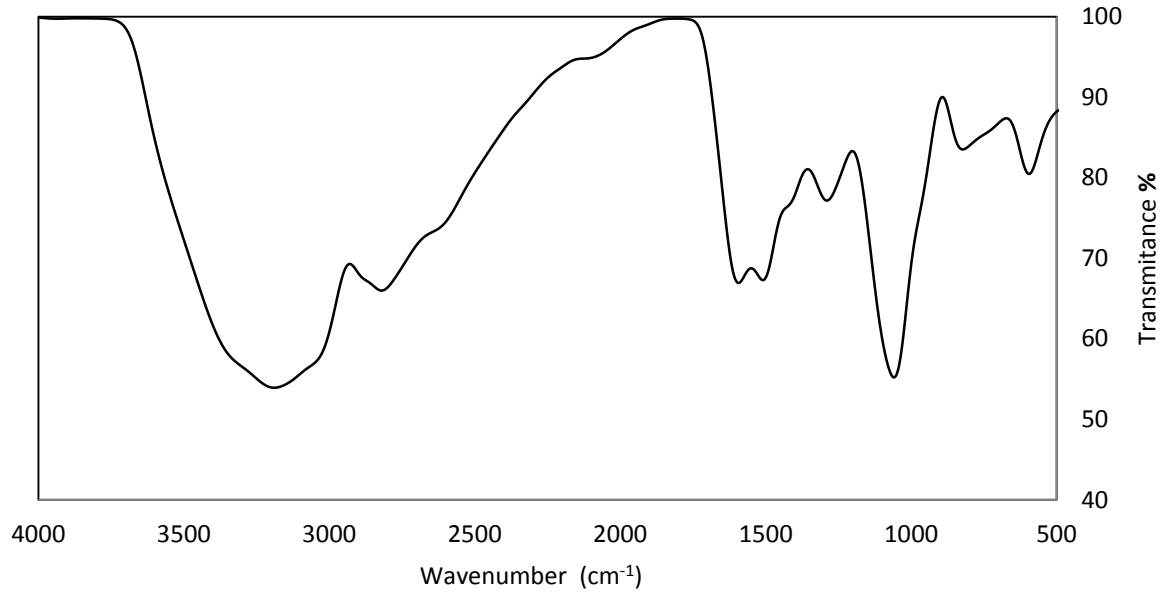

Figure 2: UV spectrum of PMAP

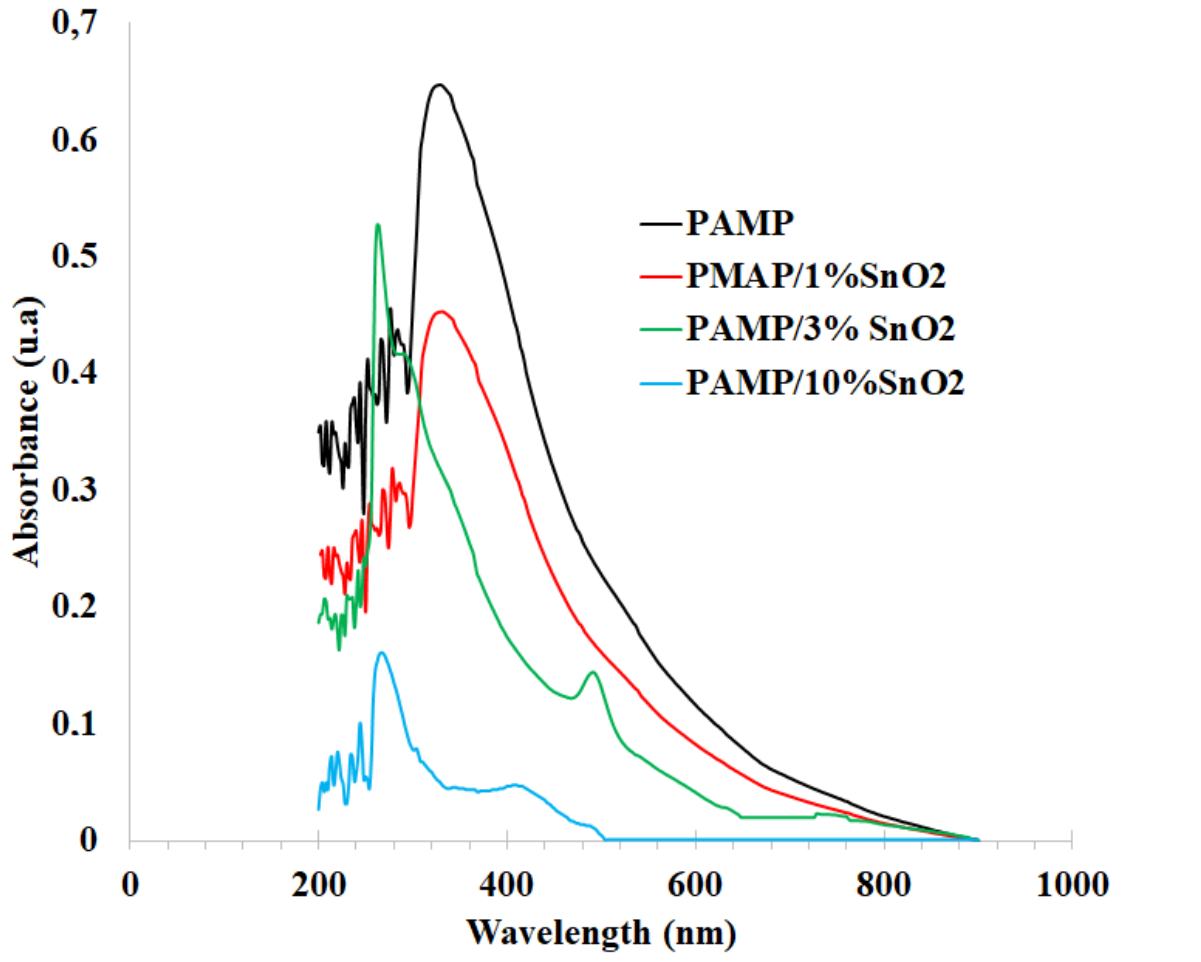

Figure 3: PMAP gap energy determined at room temperature

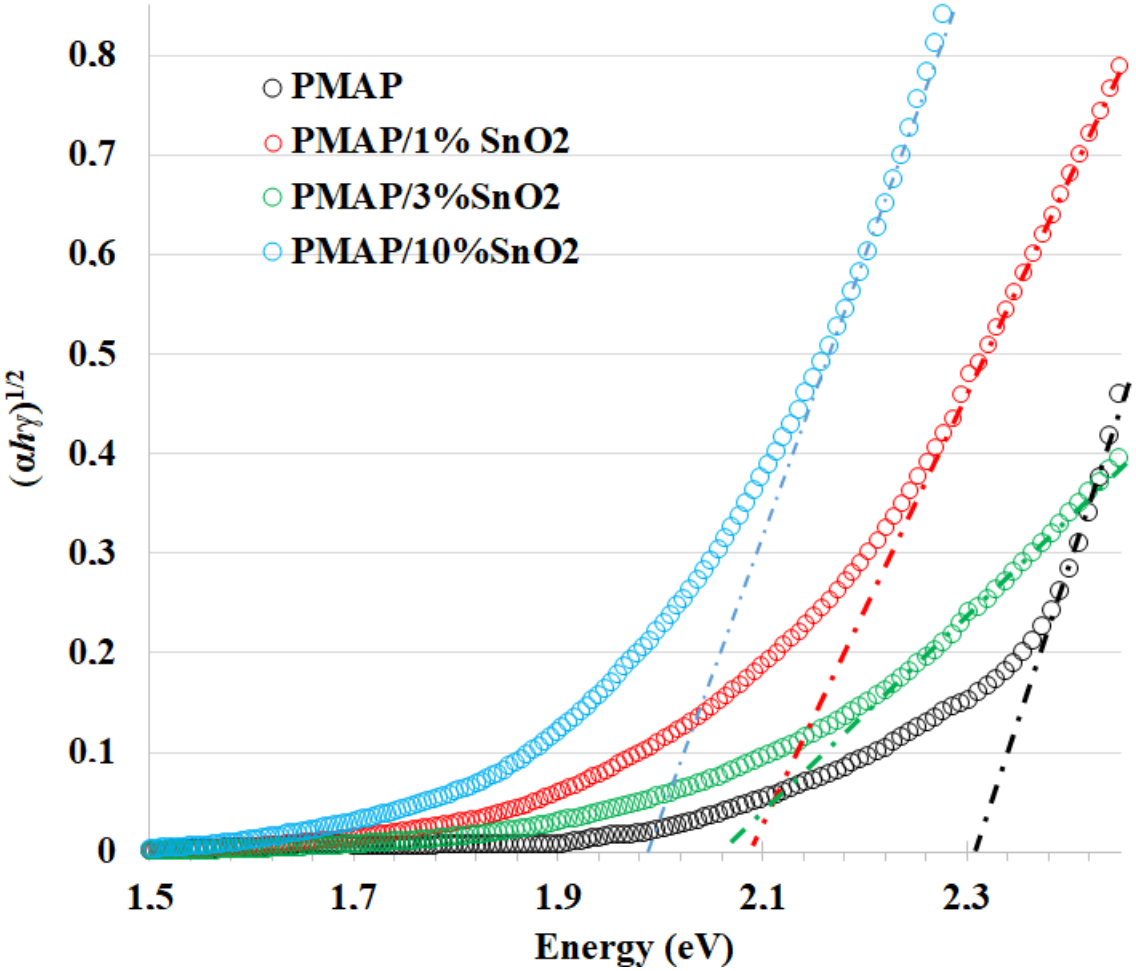

Figure. 4. X-ra y diffraction patterns of pure PMAP

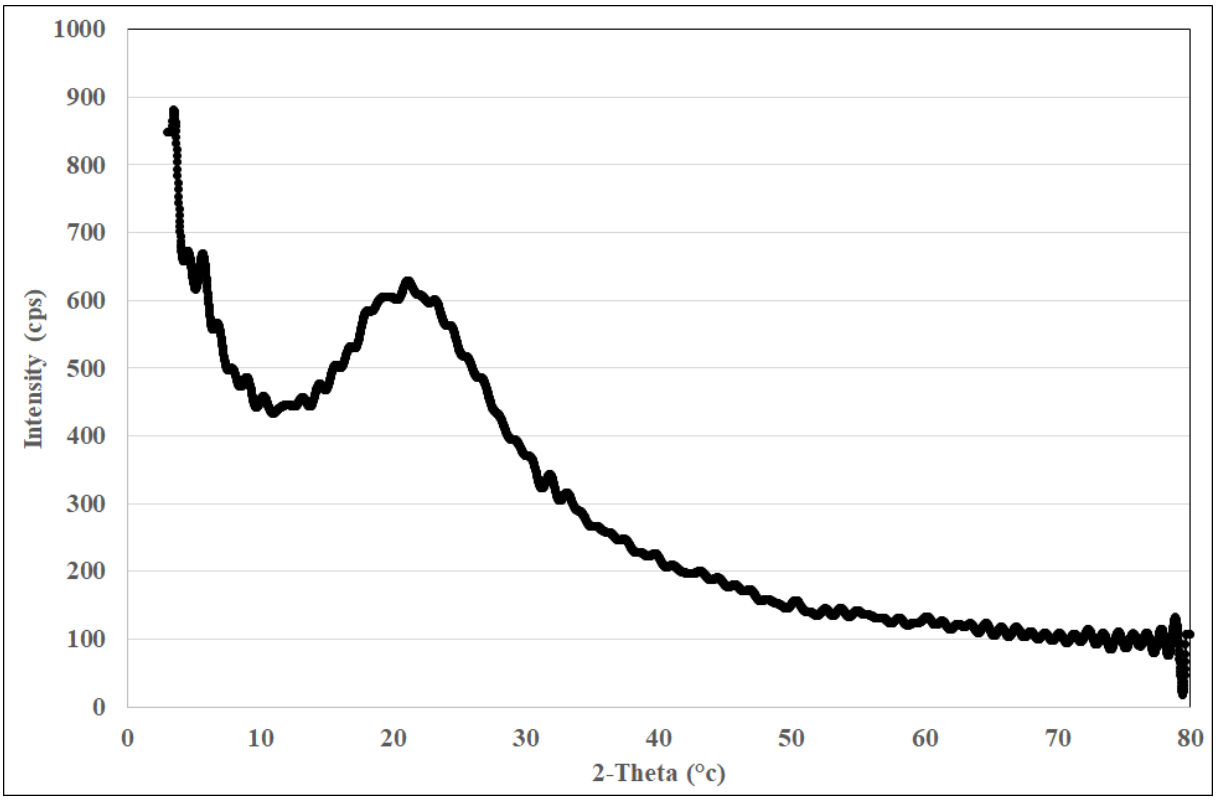

Figure. 5 X-ray diffraction patterns of SnO_2 powder

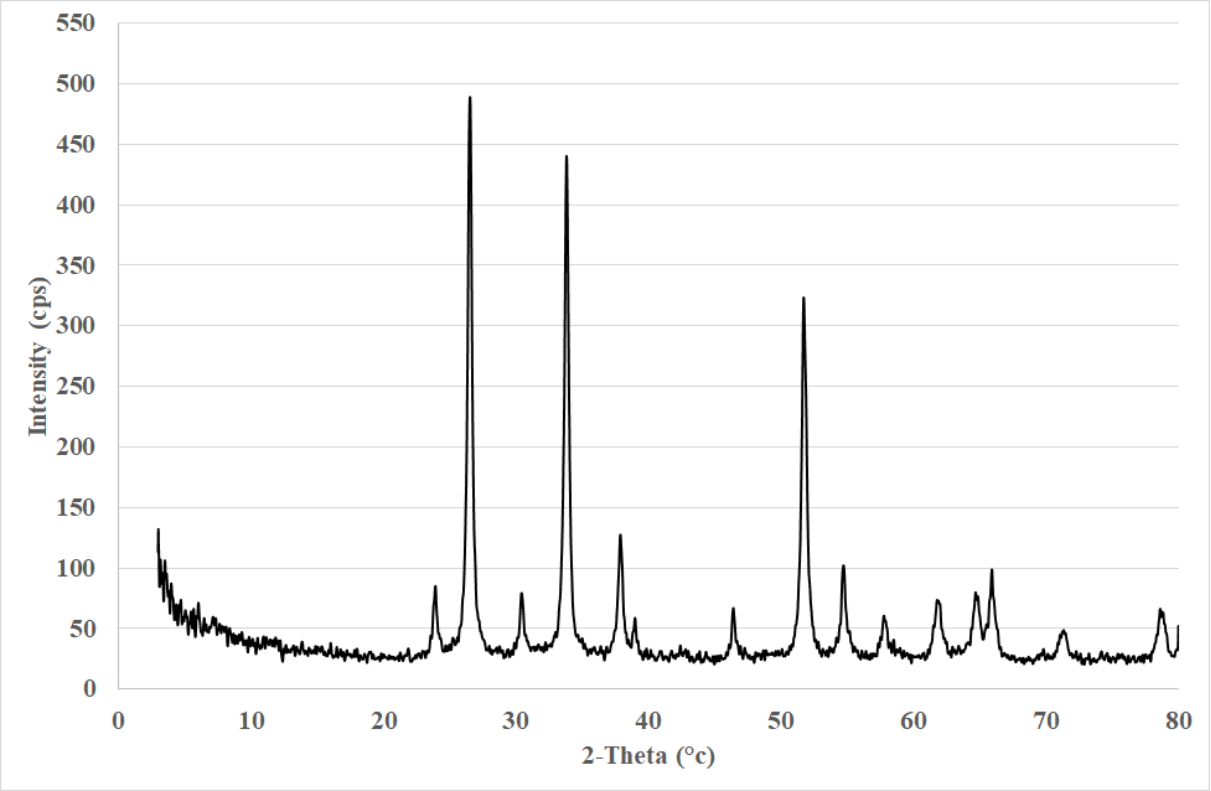

Figure.6 X-ray diffraction patterns of nanocomposites PMAP/SnO_2

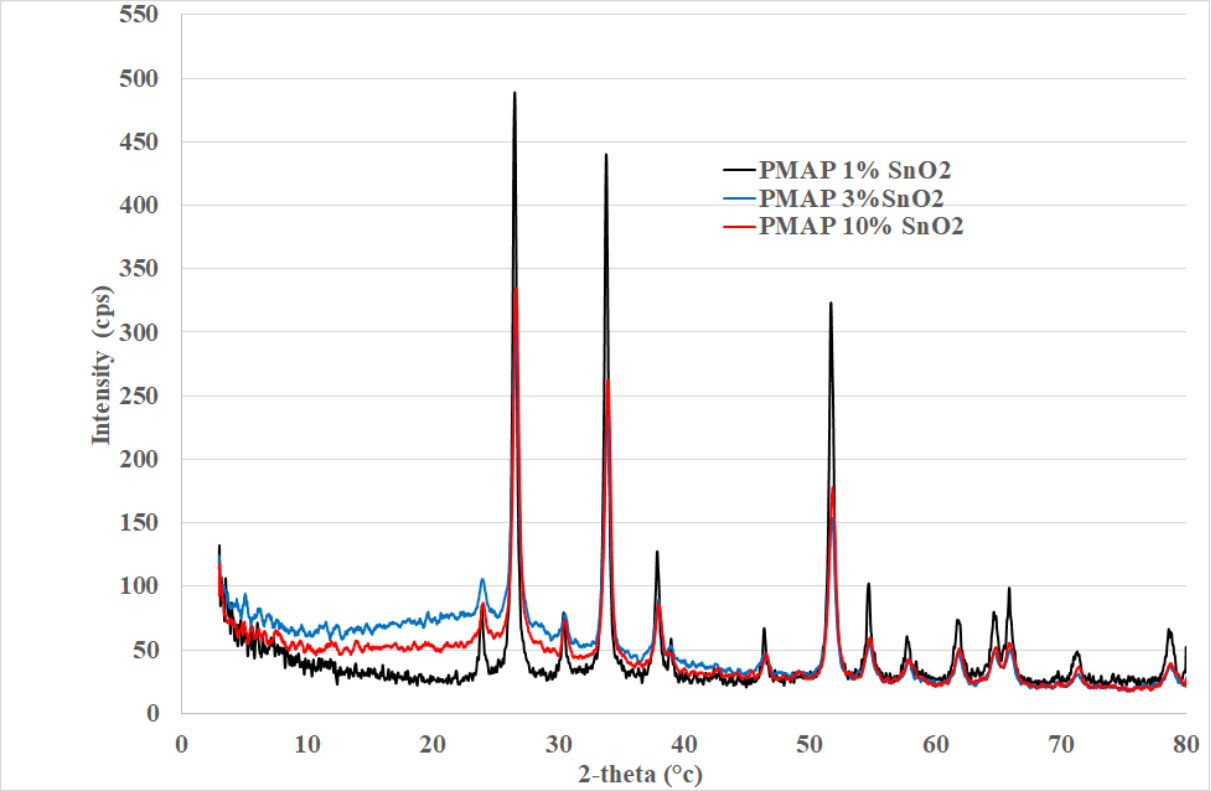

Figure 7: Arrhenius curves of the electric conductivity (Sigma) as a function of the inverse temperature at 100KHz: (1): PMAP, (2): PMAP-1%SnO_2, (3): PMAP-3% SnO_2 (3) and (4): PMAP-10% SnO_2